



Transketolase in human Müller cells is critical to resist light stress through the pentose phosphate and NRF2 pathways

Yingying Chen^{a,b}, Ting Zhang^{b,*}, Shaoxue Zeng^b, Rong Xu^{c,d}, Kaiyu Jin^e, Nathan J. Coorey^f, Yekai Wang^{c,d}, Ke Wang^g, So-Ra Lee^b, Michelle Yam^b, Meidong Zhu^{h,b}, Andrew Chang^b, Xiaohui Fan^{e,b}, Meixia Zhang^{a,i}, Jianhai Du^{c,d}, Mark C. Gillies^b, Ling Zhu^b

^a Department of Ophthalmology, West China Hospital, Sichuan University, Chengdu, Sichuan, 610041, China

^b Save Sight Institute, Faculty of Medicine and Health, The University of Sydney, Sydney, NSW, 2000, Australia

^c Department of Ophthalmology and Visual Sciences, West Virginia University, Morgantown, WV, 26506, United States

^d Department of Biochemistry, West Virginia University, Morgantown, WV, 26506, United States

^e Pharmaceutical Informatics Institute, College of Pharmaceutical Sciences, Zhejiang University, Hangzhou, Zhejiang, 310058, China

^f Canberra Health Services, Canberra, ACT, 2601, Australia

^g Key Laboratory of Molecular Nuclear Medicine, Jiangsu Institute of Nuclear Medicine, Wuxi, Jiangsu Province, 214063, China

^h New South Wales Tissue Bank, Sydney Eye Hospital, New South Wales Organ and Tissue Donation Service, Sydney, NSW, 2000, Australia

ⁱ Macular Disease Research Laboratory, Department of Ophthalmology, Sichuan University, West China Hospital, Chengdu, Sichuan, 610041, China

ARTICLE INFO

Keywords:

Transketolase (TKT)
Müller cells
Pentose phosphate pathway
NRF2
NQO1
Oxidative stress

ABSTRACT

The Pentose Phosphate Pathway (PPP), a metabolic offshoot of the glycolytic pathway, provides protective metabolites and molecules essential for cell redox balance and survival. Transketolase (TKT) is the critical enzyme that controls the extent of “traffic flow” through the PPP. Here, we explored the role of TKT in maintaining the health of the human retina. We found that Müller cells were the primary retinal cell type expressing TKT in the human retina. We further explored the role of TKT in human Müller cells by knocking down its expression in primary cultured Müller cells (huPMCs), isolated from the human retina (11 human donors in total), under light-induced oxidative stress. TKT knockdown and light stress reduced TKT enzymatic activities and the overall metabolic activities of huPMCs with no detectable cell death. TKT knockdown restrained the PPP traffic flow, reduced the expression of NAD(P)H Quinone Dehydrogenase 1 (NQO1), impaired the antioxidative response of NRF2 to light stress and aggravated the endoplasmic reticulum (ER) stress. TKT knockdown also inhibited overall glucose intake, reduced expression of Dihydropyrimidine dehydrogenase (DLD) and impaired the energy supply of the huPMCs. In summary, Müller cell-mediated TKT activity plays a critical protective role in the stressed retina. Knockdown of TKT disrupted the PPP and impaired overall glucose utilisation by huPMCs and rendered huPMCs more vulnerable to light stress by impairing energy supply and antioxidative NRF2 responses.

1. Introduction

Müller cells, specialised radial glial cells, are the primary glial cell in the retina. The primary processes of the Müller cell span the entire thickness of the neural retina, from the inner to the outer limiting membrane [1]. Müller cells perform diverse functions in the retina, including maintaining water and electrolyte balance, regulating synaptic activity, maintaining mechanical tissue homeostasis, neurovascular coupling and, possibly, neuro-regeneration. Müller cells provide both trophic and antioxidative support to photoreceptors and

neurons. All this maintains retinal homeostasis with relief of oxidative stress [2].

Müller cells actively participate in the pathogenesis of prevalent and diverse retinal diseases [3]. These include, but are not limited to, retinal detachment [4], diabetic retinopathy (DR) [5], age-related macular degeneration (AMD) [6], immunologic retinal diseases [7] and Type 2 Macular Telangiectasia [8]. Müller glia are among the first retinal cell types to exhibit metabolic changes in retinal diseases [9]. Recent reports suggest Müller cells are the primary sites of *de novo* synthesis of serine and glutathione in the neural retina, supporting neurons and protecting

* Corresponding author.

E-mail address: ting.zhang@sydney.edu.au (T. Zhang).

<https://doi.org/10.1016/j.redox.2022.102379>

Received 1 June 2022; Received in revised form 17 June 2022; Accepted 19 June 2022

Available online 24 June 2022

2213-2317/© 2022 The Authors. Published by Elsevier B.V. This is an open access article under the CC BY-NC-ND license (<http://creativecommons.org/licenses/by-nc-nd/4.0/>).

them from oxidative stress [10]. The disturbance of homeostasis caused by the malfunction of Müller glia may contribute to the elevated retina stress level.

The Pentose Phosphate Pathway (PPP), an offshoot of the glycolytic pathway, plays critical metabolic and non-metabolic roles essential for cell survival. It generates nicotinamide adenine dinucleotide phosphate (NADPH), which combats retinal oxidative stress by maintaining the appropriate reducing environment [11]. PPP is the primary retinal source of NADPH, in addition to pathways linked to mitochondria [12]. PPP plays a critical role in cellular energy supply, branching from glucose 6-phosphate (G6P), producing NADPH and ribose 5-phosphate (R5P), while also shunting carbon atoms back to the glycolytic or gluconeogenic pathway [13].

Transketolase (TKT) is a critical enzyme in the non-oxidative branch of the PPP [14] that bridges the PPP and glycolysis [15]. TKT transfers two carbon units from xylulose-5-phosphate (Xu5P) to ribose-5-phosphate, generating sedoheptulose-7-phosphate (S7P) and glyceraldehyde-3-phosphate (G3P). TKT can also transfer two carbon units from Xu5P to erythrose-4-phosphate (E4P), yielding fructose-6-phosphate (F6P) and G3P. F6P can either be used for glycolysis or be converted back to G6P to replenish the oxidative PPP. G3P can also be utilised in glycolysis, depending on cellular requirements. TKT also has non-enzymatic functions that participate in the development of hepatocarcinoma [16], the outcomes of ovarian cancer patients [17] and the metastasis of breast cancer [18]. However, the role of TKT in the retina is unknown. Here we report that TKT is almost exclusively expressed by Müller glia in the human neural retina, and TKT-dependent PPP function is crucial for the health of the Müller cells.

2. Materials and methods

Ethics: The protocols for human retina studies were approved by the Human Research Ethics Committee of the University of Sydney (HREC#:16/282) and the University of Sydney Institutional Biosafety Committee (21E011). Consent was obtained for experimentation on human tissue. The donors were 41–79 years old and the post-mortem delay times were between 15 and 36 h (see supplementary file S2).

Vibratome sectioning: Retinal punches (5 mm diameter) were fixed in 4% PFA in PBS for 1 h at room temperature before being transferred to fresh PBS. The retina punches were then embedded in 3% low-melting agarose (Lonza, Rockland, ME, 50,100) in PBS before sectioning at a 100 µm thickness using a vibratome (Leica, Germany, VT1200S). These sections were stored in 48-well cell culture plates (Corning, NY, 3548) in PBS at 4 °C until use.

Immunostaining: For vibratome sections, tissue sections were blocked with 5% normal goat serum and 1% Triton X-100 in PBS in 48-well cell culture plates at 4 °C overnight, followed by primary antibody incubation for four days at 4 °C. The tissue samples were incubated with species-specific secondary antibodies, conjugated to Alexa Fluor 488 and 594 for two days at 4 °C. The primary and secondary antibodies were diluted in PBS containing 1% normal goat serum and 1% Triton X-100. Nuclei were stained with Hoechst 33342. After thorough washing, the vibratome sections were mounted onto polylysine glass slides in Vectashield Antifade Mounting Medium (Vector Laboratories, Burlingame, CA, H-1000) and then cover-slipped. Fluorescence was detected with a confocal microscope (Zeiss, Germany, LSM 700) equipped with 405-, 488-, and 555-nm lasers. The contrast and brightness of the images were adjusted using Zen Software, Black Edition (ZEN Digital Imaging for Light Microscopy from Zeiss, Germany). Slides were defrosted for human retinal cryosections and blocked with 5% normal goat serum and 0.5% Triton X-100 in PBS at room temperature for 1 h. The slides were then washed with PBS and incubated with the primary antibodies at 4 °C overnight. The slides were washed with PBS and incubated with secondary antibodies the next day at room temperature for 4 h. The primary and secondary antibodies were diluted in PBS containing 1% normal goat serum and 0.5% Triton X-100. Nuclei were stained with Hoechst

33342. The slides were mounted and images were acquired as described. The primary antibodies used were TKT (Novus, Littleton, CO, NBP1-87441, 1:200 dilution), CRALBP (Abcam, UK, 15,051, 1:500 dilution), GFAP (Abcam, UK, ab53554, 1:500 dilution). Cells were seeded in EZ SLIDE (Millicell, Germany, PEZGS0816) for huPMCs staining and treated before being ready for immunostaining. The cell culture medium was removed. The cells were then washed twice with PBS and fixed with 2% PFA for 60 min at room temperature. After washing with PBS twice, the cells were blocked with 5% normal goat serum and a 0.5% Triton X-100 in PBS for 1 h at room temperature. The cells were then incubated with *anti*-TKT (1:50 dilution) and *anti*-GS (Millipore, Burlington, MA, MAB302, 1:50 dilution) antibodies overnight at 4 °C. The cells were then washed with PBS three times and incubated with secondary antibodies (Alexa Fluor 488 and Alexa Fluor 594) for 2 h at room temperature. Primary and secondary antibodies were diluted in 1% goat serum and a 0.5% Triton X-100 in PBS. After this, the cells were washed with PBS three times and incubated with Hoechst 33342 for 5 min. The cells were washed with PBS three times. The walls of the EZ SLIDE were broken, as described in the manual. The slides were mounted, and the images were acquired as described.

Western Blot: Proteins were collected by RIPA buffer (Sigma-Aldrich, St. Louis, MO, R0278) with protease/phosphatase inhibitor (Cell Signalling Technology, Danvers, MA, 5872S). Total proteins were mixed with NuPAGE loading dye and reducing buffer (Life Technologies, Carlsbad, CA) and heated for 10 min at 70 °C. The supernatants were loaded onto the NuPAGE 4–12% Tris-Bis gels (Life Technologies). Proteins were separated by electrophoresis at a constant 180 V at 4 °C for 70 min. The gels were transferred onto polyvinylidene difluoride membrane (PVDF, Millipore, Burlington, MA) at a constant 100 V at 4 °C for one and a half hours. The membranes were incubated in 5% bovine serum albumin (BSA) in Tris-buffered Saline with 0.1% Tween 20 (TBST) for 1 h to block non-specific binding. The following primary antibodies were used: α, β-Tubulin (Cell Signalling Technology, 2148, 1:1000 dilution), Transketolase (Novus, Littleton, CO, NBP1-87441, 1:500 dilution), GAPDH (Cell Signalling Technology, 2118, 1:1000 dilution), NQO1 (Abcam, UK, ab34173, 1:2000 dilution), DLD (Proteintech, Rosemont, IL, 16431-1-AP, 1:2000 dilution), IRE1α (Cell Signalling Technology, 3294, 1:1000 dilution) and pIRE1α (Novus, NB100-2323, 1:1000 dilution). After extensive washing, protein expression was visualised using ECL (Biorad, Hercules, CA, 170–5061) and quantified with the Gene Tools image scanning and analysis package.

Human primary Müller cells (huPMCs) culture: huPMCs were cultured as previously described [19]. Briefly, the human retina was collected in a yellow sterile tube containing 5 mL DMEM (Gibco, Amarillo, TX, 10569). All DMEM below was this unless otherwise mentioned. The tube was wrapped in foil to avoid light and kept in the cold room overnight. On the next day, the retina tissue was digested in TrypLE™ (Invitrogen, Waltham, MA, 12563–029) for 1 h in a cell culture incubator. Digestion was terminated by the complete culture medium (DMEM + 10% fetal bovine serum (FBS, Sigma-Aldrich, F9423) + 1% Penicillin-Streptomycin (Sigma-Aldrich, P4333)). The tissue was then cut into small pieces and transferred to a T25 cell culture flask (Corning, 3289). The small pieces were nailed to the bottom of the flask by needles and covered with 2 mL complete culture medium. Another 2 mL fresh complete culture medium was added to the flask one week later. The huPMCs were maintained by changing the medium twice a week. The huPMCs usually grew out of the retina pieces in two-four weeks.

siRNA transfection: huPMCs were cultured and passaged to P2 before seeding. On day 0, P3 huPMCs were seeded in cell culture plates. The densities were as follows: 4000 cells per well in 96-well plates (Corning, 3340); 20,000 cells per well in 24-well plates (Corning, 3524); 40,000 cells per well in 12-well plates (Corning, 3336); 80,000 cells per well in six-well plates (Corning, 3335). On day 3, the confluency usually reached 60%–70%. The complete culture medium was changed with the transfection culture medium (DMEM + 10% FBS), and the huPMCs were transfected with either control siRNA (Ambion, 4390843) or TKT siRNA

(Ambion, 4392420, siRNA ID 14161) by lipofectamine3000 (Invitrogen, L3000-008) according to the manual. Briefly, siRNA was diluted in Opti-MEM reduced serum medium (ThermoFisher, 31985070) to the final concentration of 10 nM in each well. Lipofectamine3000 was also diluted in Opti-MEM reduced serum medium to the lowest concentration suggested in the manual. The diluted siRNA and lipofectamine3000 were mixed and incubated at room temperature for 5 min. The mixture was then added to the wells with a transfection culture medium. The cells were cultured in an incubator for three days before further treatment.

2.1. $1, 2\text{-}^{13}\text{C}_2$ glucose labelling experiment and metabolite analysis

HuPMCs were cultured and seeded in six-well plates as described above. The culture medium was changed to a labelling medium (DMEM, no glucose; Gibco, 11966) with 5 mM $1, 2\text{-}^{13}\text{C}_2$ glucose (Cambridge Isotope Lab, UK, 138079-87-5) three days after TKT siRNA treatment. The huPMCs were labelled with the tracer at 37 °C in a CO₂ incubator for 24 h. Then the metabolites were extracted with 80% methanol and analysed by gas chromatography-mass spectrometry (GC-MS) as described [20]. Molecules with different numbers of ¹³C atoms were distinguished and labelled with Mn (n: number of ¹³C). The measured distribution of the isotopologues was corrected for the natural abundance of ¹³C metabolite intensity using the IsoCor [21].

Light exposure: The light exposure devices were set in a 37 °C cell culture incubator with 5% CO₂ perfusion. An adjustable LED plate (Wuxi OcuTech, Wuxi, Jiangsu, China) was fixed at the top of a middle layer to emit white light. The plates exposed to strong light were settled at the same area straight under the LED plate, where light intensity was measured to be 32K lux. The light spectrum was shown in Fig. 2. Light intensity was measured both before and after light exposure. A temperature detector was fixed at the bottom of the same layer to monitor the temperature in system. A fan was set to facilitate airflow. Most of the time, an area in the top layer of the incubator was set to place the dim light (5 lux) control plates. For AlamarBlue and LDH assay, cells in intense light exposed and dim light control groups were seeded apart in the same 96-well plates to avoid introducing variance from different plates when reading. The control wells were wrapped with foil when exposed to light. The plates' black walls and transparent bottom allowed only light from the top to travel through the cells while blocking all reflected light from adjacent wells. Also, huPMCs were incubated with a starving culture medium (DMEM +1% FBS + 1% Penicillin-Streptomycin) overnight before exposure to light.

TKT activity assay: P3 huPMCs were seeded in six-well plates and treated with siRNA and light, as described above. The assay was conducted following the manual of the Transketolase Activity Assay Kit (Fluorometric) (BioVision, Milpitas, CA, K2004-100). Briefly, 50 µL TKT Assay Buffer was used in each well of a six-well plate to lyse the huPMCs. The lysates were collected and centrifuged at 10,000 g and 4 °C for 15 min. Then, the supernatants were transferred to new clean tubes, and protein concentrations were calculated by QuantiPro™ BCA Assay Kit (Sigma-Aldrich, QPBCA). For each sample, 1 µg protein was used in one assay reaction. The reactions were performed in the white flat bottom 384 well plates (Corning, 3572). Measurements were immediately started with a plate reader (Safire, Tecan, Switzerland), recording fluorescence at Excitation/Emission 535/587 nm at 5 min intervals for 45 min at 37 °C. Calculations were conducted according to the manual. The definition of the unit was that one unit of transketolase is the amount of enzyme that produces 1 µmol of G3P per minute at pH 7.5 at 37°C.

AlamarBlue assay and LDH assay: P3 huPMCs were seeded in 96-well plates and treated with siRNA and light, as described above. Medium in the wells was replaced with starving culture medium containing 10% of AlamarBlue reagent (ThermoFisher, DAL1100) and incubated in a cell culture incubator. Fluorescence was detected hourly, according to the manual. The replaced medium was used for LDH assay using Pierce

LDH Cytotoxicity Assay Kit (ThermoFisher, 88954). Briefly, the reaction mix in the kit was prepared according to the instruction. Supernatants collected from the replaced medium were mixed with the same amount of reaction mix in a 384-well plate (Corning, 3680) and incubated at room temperature for 30 min. According to the manual, absorbance was detected using a plate reader (Safire, Tecan).

NADPH/NADP + ratio Assay and ATP assay: P3 huPMCs were seeded in 24-well plates and treated with siRNA and light as described above. The NADPH/NADP + ratio assay was conducted following the manual of the NADP/NADPH-Glo™ Assay (Promega, Madison, WI, G9081). Briefly, the medium in the wells was replaced with 60 µL PBS. 60 µL lysis buffer (0.2 N NaOH with 1%DTAB) was added to each well to lyse the cells. The lysates were homogenised and centrifuged to get supernatants. NADPH levels and NADP + levels in the supernatant were detected individually: to measure NADP+, 15 µL 0.4 N HCl was mixed with 30 µL supernatants and heated at 60 °C for 15 min before 15 µL f Trizma® base was added; to measure NADPH, 30 µL supernatants were heated at 60 °C for 15 min before 30 µL HCl/Trizma solution was added. Luciferin Detection Reagent was prepared according to the manual. 10 µL treated supernatants were mixed with 10 µL detection reagent in each well in a 384-well plate (Corning, 3572). Readings for NADPH and NADP+ were acquired by a plate reader (CLARIOstar), respectively, and NADPH/NADP + ratio was calculated accordingly. ATP assay was conducted following the fluorometric manual of the ATP Colorimetric/Fluorometric Assay Kit (Sigma-Aldrich, MAK190). Briefly, to prepare a sample, cells in each well were lysed with 100 µL ATP assay buffer and deproteinised by a 10 kDa MWCO spin filter (Sartorius, Germany, VS0102). 0.01 mM ATP standard solution was used to generate standards. Samples and standards were mixed with the reaction mix prepared from the kit in a 384-well plate (Corning, 3680). Part of the samples was separated and mixed with sample blank mix. After incubation for 30 min at room temperature, fluorescence was detected by the plate reader (Safire, Tecan), and the ATP level was calculated accordingly.

RNA sequencing: total RNA was extracted from treated huPMCs using GenElute™ Single Cell RNA Purification Kit (Sigma-Aldrich, RNB300). A total amount of 1 µg RNA per sample was used as input material for the RNA sample preparations. Sequencing libraries were generated using NEBNext® Ultra™ RNA Library Prep Kit for Illumina® (NEB, USA) following the manufacturer's recommendations, and index codes were added to attribute sequences to each sample. To select cDNA fragments of preferentially 150–200 bp in length, the library fragments were purified with the AMPure XP system (Beckman Coulter, Beverly, USA). Then 3 µL USER Enzyme (NEB, USA) was used with size-selected, adaptor-ligated cDNA at 37 °C for 15 min followed by 5 min at 95 °C before PCR. Then PCR was performed with Phusion High-Fidelity DNA polymerase, Universal PCR primers and Index (X) Primer. Finally, PCR products were purified (AMPure XP system), and library quality was assessed on the Agilent Bioanalyzer 2100 system. According to the manufacturer's instructions, the clustering of the index-coded samples was performed on a cBot Cluster Generation System using PE Cluster Kit cBot-HS (Illumina). After cluster generation, the library preparations were sequenced on an Illumina platform, and paired-end reads were generated. RNAseq data are available at <https://www.ncbi.nlm.nih.gov/geo/query/acc.cgi?acc=GSE198554>.

RNA data analysis: Raw data (raw reads) of FASTQ format were first processed through fastp. In this step, clean data (clean reads) were obtained by removing reads containing adapter and poly-N sequences and reads with low quality from raw data. At the same time, Q20, Q30 and GC content of the clean data were calculated. All the downstream analyses were based on clean data with high quality. Reference genome and gene model annotation files were downloaded from the genome website browser (NCBI/UCSC/Ensembl) directly. Paired-end clean reads were aligned to the reference genome using the Spliced Transcripts Alignment to a Reference (STAR) software. FeatureCounts was used to count the read numbers mapped of each gene. And then RPKM of each

gene was calculated based on the length of the gene and read counts mapped to this gene. Differential expression analysis between two conditions/groups (three biological replicates per condition) was performed using the DESeq2 R package. Genes with a P-value < 0.05 found by DESeq2 were assigned as differentially expressed.

QIAGEN Ingenuity Pathway Analysis (QIAGEN IPA) was used to study the functional changes after the treatments. Ingenuity canonical pathways with a p-value less than 0.05 and zScore no less than 2 were considered significant.

Human retinal explant culture: human retinal explants were cultured as previously described [20]. The human retina was dissected. 3 mm and 4 mm diameter retinal pieces were trephined with biopsy punches. The retinal explants were transferred to 12-well plates (Corning, 3513) equipped with cell culture inserts (Corning, 3460). The basic culture medium for the retinal explants was modified from the commercial culture medium but was thiamine-free. A detailed formulation of the thiamine-free medium was provided in a supplementary file (S3). The thiamine free medium was supplemented with 2% B27 (Gibco, 17,504), 1% N2 (Gibco, 17,502), 1% ITS-X (Gibco, 51,500) and 1% GlutaMax (Gibco, 35,050). Thiamine (Sigma-Aldrich, T1270) and oxythiamine (Sigma-Aldrich, O4000) were dissolved in the inorganic salt solution (see supplementary file S3) respectively and added to the culture medium to the final concentration of 12 μ M and 200 μ M. The retinal explants were cultured for 24 h in the medium before being changed to a thiamine free medium supplemented with N2, B27, ITS-X and GlutaMax, and exposed to dim or strong light for 4 h before further analysis.

TUNEL staining and quantification: vibratome sections from cultured retinal explants were stained with a TUNEL assay kit (Roche, Switzerland, 11684795910) according to the manual. Briefly, a total volume of 50 μ L Enzyme Solution was added to the remaining 450 μ L Label Solution to obtain a 500 μ L TUNEL reaction mixture. The vibratome sections were incubated in the wells of a 48-well plate, with a 125 μ L TUNEL reaction mixture in each well. The plate was sealed with parafilm and incubated in a 37 °C incubator for 1 h. Then the sections were washed with PBS and counterstained with Hoechst for 30 min. The sections were washed with PBS before being mounted as described

above for imaging. Images were taken with a confocal microscope (Zeiss, Germany, LSM 700). TUNEL + cells were quantified by ImageJ. 4–7 images for each slide were used for statistic analysis.

3. Results

3.1. TKT expression in human Müller cells in normal and diseased retina

TKT expression in the human retina was analysed by immunofluorescent staining on vibratome sections of the macula (Fig. 1A–D) and periphery (Fig. 1E–I). Human retinal sections were stained with TKT antibody (green, Fig. 1A, E) and the Müller cell marker, CRALBP antibody (red, Fig. 1B, F). TKT expression was predominately localised in the inner nuclear layer of the retina (Fig. 1C, G). The nuclei with positive TKT staining were wrapped by the CRALBP staining. This suggested the Müller cells express the TKT protein (Fig. 1I). We further explored the TKT expression in a retina from a donor with age-related macula degeneration (AMD) (Fig. S1). The AMD retinal section was stained with the Müller cell gliosis marker GFAP antibody (green, Fig. S1A) and TKT antibody (red, Fig. S1B). We found the expression of TKT significantly decreased in gliotic Müller cells (Figs. S1C and D).

3.2. The role of TKT in human Müller cells

TKT expression was further evaluated in different cells and tissues, including the human retina, human primary Müller cells (huPMCs), human embryonic kidney 293 cells (HEK293), and human extraocular muscle (Fig. 2A). TKT expression was normalised to the loading control glyceraldehyde-3-phosphate dehydrogenase (GAPDH), and the relative TKT expression level was normalised to TKT expression in the human retina (Fig. 2B). We found that both human retina and huPMCs expressed TKT. TKT expression level was high in HEK293 cells (positive control) and negligible in muscle (negative control).

TKT protein is gathered in the nucleus of the huPMCs and also distributed in the cytoplasm (Fig. 2C). TKT was further knocked down in huPMCs using siRNAs and confirmed by Western blot (Fig. 2D–E). TKT

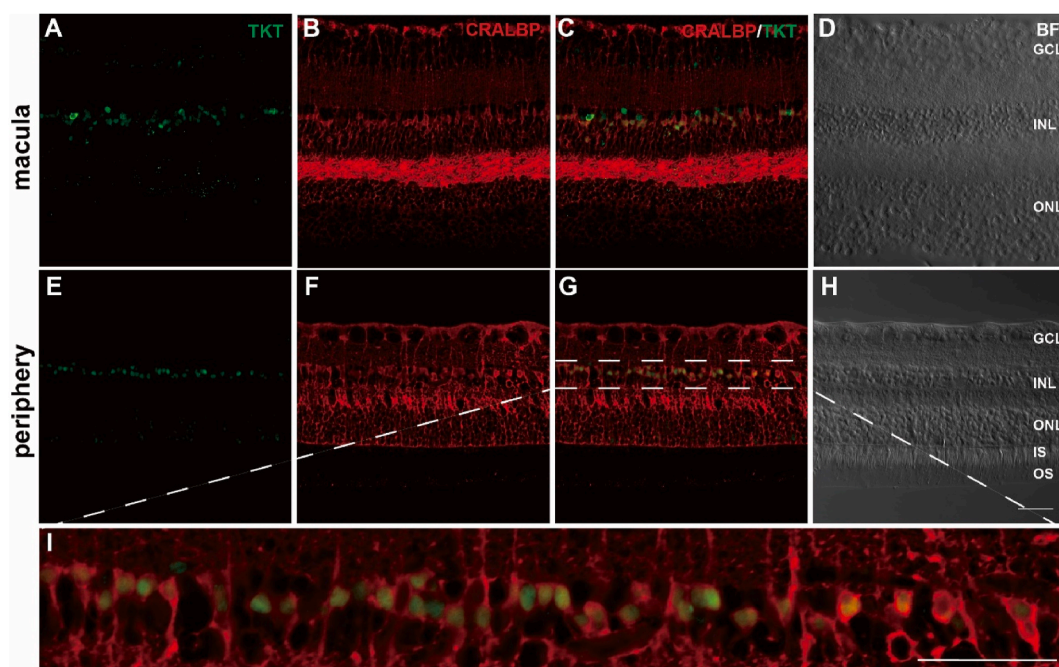


Fig. 1. TKT expression in the healthy human macula (A–D) and peripheral retina (E–I). A, B, E, F Human retina immunoreactivity for TKT (green, A and E) and CRALBP (red, Müller cell marker, B and F). C, G CRALBP and TKT double staining. D, H Bright-field images. I Field-enlarged image from G (dotted box). Both scale bars are equal to 50 μ m. BF: bright field. GCL: ganglion cell layer. INL: inner nuclear layer. IS: inner segments. ONL: outer nuclear layer. OS: outer segments. TKT: transketolase. (For interpretation of the references to colour in this figure legend, the reader is referred to the Web version of this article.)

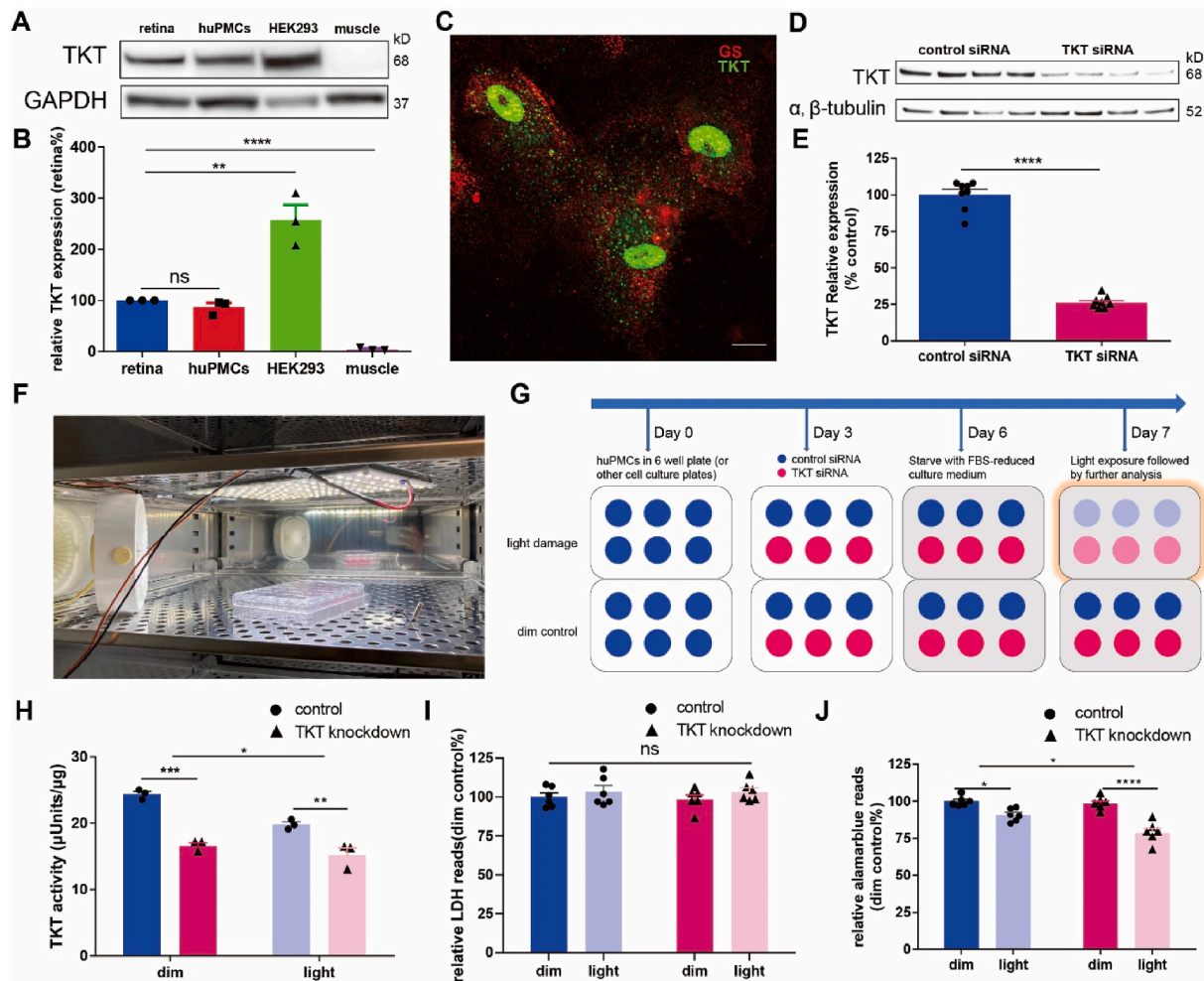


Fig. 2. *TKT function in human Müller cells.* **A** WB analysis of TKT and GAPDH in the human retina, human primary Müller cells, HEK293 cells (positive control) and human extraocular muscle (negative control). **B** Quantitative analysis of TKT expression in the cells and tissue. TKT expression level is normalised against GAPDH. **C** Immunofluorescence of huPMCs with TKT (green) and Müller cell marker GS (red) staining. Scale bar = 20 μm . **D** WB analysis of TKT and α/β tubulin in huPMCs with control siRNA or TKT siRNA treatment. **E** Quantitative analysis of TKT expression with control siRNA or TKT siRNA treatment. TKT expression level is normalised against α/β tubulin. $n = 8$ per group. Error bars = SEM. **F** Light exposure apparatus within the cell culture incubator. **G** Experimental design schematic of light exposure following TKT knockdown: third passage (P3) huPMCs were seeded on day 0 and treated with siRNAs treatment on day 3. Three days later, cells were starved overnight. Light exposure experiments were conducted on day 7, followed by further analysis. **H** Reduction in TKT enzymatic activity after TKT knockdown and light stress. $n = 3$ per group. Error bars = SEM. **I** LDH assay and **J** AlamarBlue assay after TKT knockdown and light stress. All reads were normalised to the average read of the dim control group. $n = 6$ per group. Error bars = SEM. All comparisons between two groups (short lines) were conducted using a *t*-test. Longline in Figures **H** and **J** indicated an interaction between TKT knockdown and light exposure detected using two-way ANOVA. Long dash in figure **I** indicated no significant difference between all four groups. ns: not statically significant; *: $p < 0.05$; **: $p < 0.01$; ***: $p < 0.001$; ****: $p < 0.0001$. Errors bars = SEM. CRALBP: Cellular retinaldehyde-binding protein. GAPDH: Glyceraldehyde 3-phosphate dehydrogenase. huPMCs: human primary Müller cells. LDH: Lactate dehydrogenase. siRNA: small interfering RNA. TKT: transketolase. WB: Western blot. (For interpretation of the references to colour in this figure legend, the reader is referred to the Web version of this article.)

siRNAs reduced TKT protein level in huPMCs to 20–30% relative to negative control siRNAs. We used intense light to mimic the stress in the AMD retina. Light stress was applied to cultured huPMCs with or without TKT knockdown (apparatus in Fig. 2F) to explore the correlation between TKT dysregulation and stress in huPMCs. HuPMCs were exposed to light stress for 4 h (32k lux, white light, spectrum in Fig. S2), with dim light (5 lux) as controls (see methods and flowchart (Fig. 2G) for device details). TKT activity levels were assessed in different treatment groups to investigate how siRNA knockdown and light stress affected TKT activities in Müller cells. TKT activity was significantly reduced by TKT siRNA treatment, irrespective of whether light stress was applied (Fig. 2H). Two-way ANOVA analysis found that the interaction between TKT knockdown and light stress also contributed to the significant variance between the four groups (Fig. 2H). Light stress had a negative effect on enzyme activity. Intriguingly, 20–30% of residual TKT

performed about 70% of the enzyme activities following siRNA knockdown, with or without light stress.

LDH assays were performed to assess whether decreased TKT activity resulted from cell death. Increased LDH activity is a sensitive assay for cell death, as dead cells release their intracellular LDH into the media. LDH activity levels were similar in the control and treated groups (Fig. 2I). AlamarBlue assay was used to evaluate the overall metabolic activity of huPMCs after treatments (Fig. 2J). The AlamarBlue assay indicates the rates of reducing resazurin to resorufin (a highly fluorescent red compound), thus demonstrating the reducing power of living cells originating from their metabolic activities. Light stress reduced the metabolic activity of huPMCs by 10% compared with dim light controls. The reduction was doubled to around 20% when TKT was knocked down simultaneously.

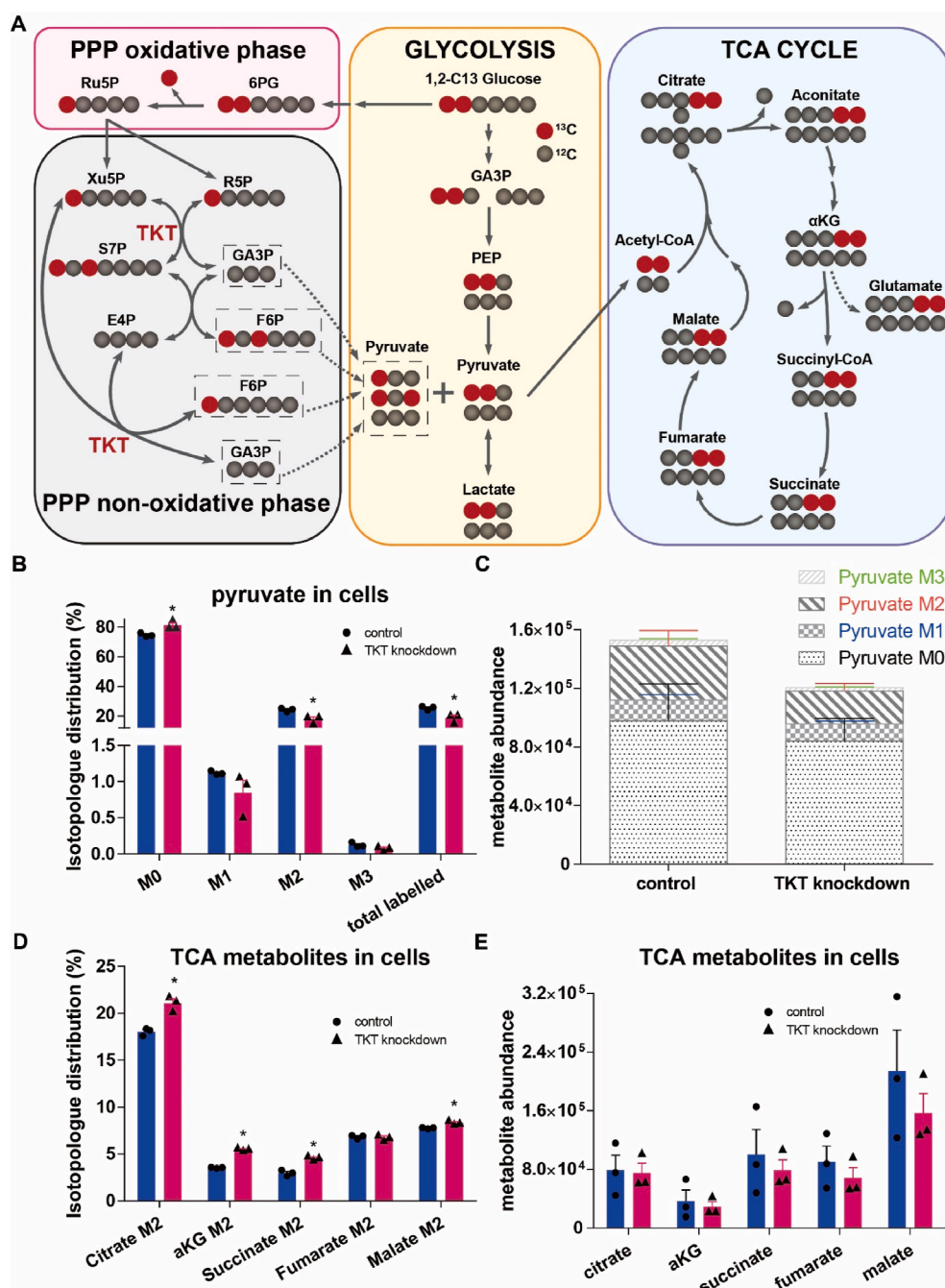
3.3. Metabolic analysis of huPMCs following TKT knockdown

1, 2-¹³C glucose was used as a tracer to evaluate glucose metabolism through PPP and glycolysis, as metabolites from PPP are labelled with one ¹³C, while glycolytic metabolites incorporate two ¹³C units. HuPMCs were treated with TKT siRNA or control siRNA for three days before being labelled with the tracer for 24 h. Nineteen metabolites and their isotopologues from labelled cells and culture medium were detected by gas chromatography-mass spectrometry (**supplementary file S1**). A schematic of labelled metabolic intermediates is shown: 1, 2-¹³C glucose can enter the glycolytic pathway (yellow block) or the PPP (pink and grey blocks, respectively) (**Fig. 3A**). TKT controls conversion between the sugars (glyceraldehyde 3-phosphate (GA3P), erythrose 4-phosphate (E4P), ribose 5-phosphate (R5P), xylulose 5-phosphate (Xu5P), fructose 6-phosphate (F6P), sedoheptulose 7-

phosphate (S7P)) in the non-oxidative phase of PPP, potentially providing GA3P and F6P for glycolysis. Since it was very unlikely that M2 metabolites would be derived from PPP, or M1 metabolites from glycolysis, under our culture conditions, we believe that the M1 pyruvate was derived from the PPP only and the TCA M2 metabolites were generated from the first glycolytic cycle.

The effect of TKT knockdown on pyruvate synthesis was assessed by comparing isotopologue distribution of labelled and unlabelled pyruvate between control and TKT knockdown huPMCs (**Fig. 3B**). The enrichment of M1 pyruvate, mainly synthesised from PPP, decreased after TKT knockdown, with total labelled pyruvate also decreasing. M1 pyruvate detected in the medium also decreased after TKT knockdown (**Fig. S3A, B**). In addition, TKT knockdown decreased the abundance of all pyruvate isotopologues (**Fig. 3C**).

M2 metabolites in TCA cycle intermediates mainly were derived



from glycolysis. Upon TKT knockdown, the enrichment (proportion) of M2 TCA cycle metabolites was higher (Fig. 3D), but the total pools of TCA cycle metabolites were reduced (Fig. 3E), suggesting that TKT is critical to control the shunting of glucose for mitochondrial oxidation.

3.4. Transcriptomic analysis of huPMCs following TKT knockdown and light stress

TKT is active in diverse signalling pathways, including the NRF2 [13] and EGFR pathways [16]. Transcriptomic analysis was performed on RNA extracted from huPMCs following siRNA and light treatments. Twelve samples from three donors were analysed, each containing four groups, including “dim control” (DC), “dim knockdown” (DK), “light control” (LC), and “light knockdown” (LK). Significant expression changes of differentially expressed genes (DEGs) were observed, by clustered heatmap, between stress and non-stressed groups (Fig. 4A). Transcriptomic differences between TKT knockdown and control groups were consistent between the donors, except for R09_LC, likely due to inter-individual differences.

A volcano plot (Fig. 4B) was used to study the overall distribution of DEGs in huPMCs after TKT knockdown. TKT knockdown efficiency was validated as TKT mRNA had the most significant fold downregulation in the “DK vs DC” volcano plot (Fig. 4B). We also showed the “LK vs LC” volcano plot in the supplementary figure (Fig. S4A). A co-expression Venn diagram visualised the DEGs that participated in the huPMC in response to light stress, with or without TKT knockdown (Fig. 4C). 138 DEGs belonged to both “LC vs DC” and “LK vs DK”, while 289 DEGs were unique to “LC vs DC” and 28 were unique to “LK vs DK” (Fig. 4C). We also made the Venn diagram comparing “DK vs DC” DEGs and “LK vs LC” DEGs in the supplementary figure (Fig. S4B).

Functional changes in response to light stress after TKT knockdown and associated signalling pathways in “LC vs DC” (Fig. 4D) and “LK vs DK” (Fig. 4E) were investigated using QIAGEN Ingenuity Pathway Analysis (IPA). Five pathways were activated after light stress regardless of the expression levels of TKT, including the NRF2-mediated oxidative stress response, the unfolded protein response, the endoplasmic reticulum stress pathway, ERK5 signalling and the coronavirus pathogenesis pathway. There were also pathways directly related to TKT expression level. For example, the Superpathway of Cholesterol Biosynthesis was only activated when TKT expression was normal, while iNOS signalling was only activated when TKT was knocked down. These results suggest that TKT levels govern the responses of huPMC to light stress. The most significantly activated pathway in “LK vs DK”, NRF2-mediated oxidative stress response, was analysed in more detail. Analysis of classical NRF2-related DEGs and their associated reads (Fig. 4F) found that several oxidative stress response genes (NRF2, DNAB1, HMOX1, TXNRD1) were less robustly activated by light stress following TKT knockdown. The information about the signalling pathways enriched in “DK vs DC” and “LK vs LC” by IPA is provided in the supplementary file S5.

3.5. NQO1, DLD and anti-oxidation responses

The transcriptomic analysis suggested that the NRF2 pathway was activated in huPMCs exposed to light stress. One of the key genes in the NRF2 pathway, NQO1, had significant transcriptional changes in different treatment groups (Fig. 5A). NQO1 mRNA was elevated in normal huPMCs after light exposure, and it was reduced compared with control cells after TKT knockdown. HuPMCs with TKT knockdown had less NQO1 protein, as quantified by Western blot than control huPMCs (Fig. 5B and C), consistent with the transcriptomic analysis. HuPMCs tended to have decreased expression of NQO1 protein following light stress exposure. In contrast, huPMCs with TKT knockdown exposed to light had the lowest NQO1 expression level among non-treatment control, TKT knockdown and light stress groups.

Both NQO1 downregulation and PPP inhibition may disrupt the cellular generation of NADPH. Therefore, the NADPH/NADP⁺ ratio in

the cells was analysed to study the redox state (Fig. 5D). Light exposure significantly reduced the NADPH/NADP⁺ ratio. Although there was no significant decrease in the NADPH/NADP⁺ ratio after TKT knockdown, the combined treatment of TKT knockdown and light stress significantly decreased the ratio of NADPH/NADP⁺ as indicated by a two-way ANOVA analysis.

The transcriptional level of dihydrolipoamide dehydrogenase (DLD), a glucose metabolism-related gene, was significantly changed in huPMCs after TKT knockdown (Fig. 5E). DLD protein expression was decreased, independent of light stress (Fig. 5F and G). Light stress reduced ATP levels and the NADPH/NADP⁺ ratio in huPMCs (Fig. 5D, H). ATP levels were significantly lower after light exposure when TKT was knocked down in huPMCs than in controls with normal TKT expression. The interaction between TKT knockdown and light stress also contributed to the significant variance. These results suggest that TKT performs a crucial role in retinal anti-oxidation and energy supply.

3.6. TKT was critical for ER stress responses and cell survival in the human retina

The IPA analysis also suggested that light stress and TKT knockdown (Fig. 4D and E) exacerbated stress in the ER. We assessed the expression of the ER stress marker, inositol requiring enzyme-1 α (IRE1 α) [22] in the huPMCs with or without TKT knockdown under the light stress, and compared the expression of phosphorylated IRE1 α (pIRE1 α) with IRE1 α . We found that light stress induced the expression of pIRE1 α , and TKT knockdown further increased the expression of pIRE1 α (Fig. 6A and B), suggesting that TKT knockdown aggravates ER stress induced by the light stress.

We further explored the effect of inhibiting TKT under stress on the phenotype of the human retina. Oxythiamine was used to inhibit TKT in human retinal explants cultured in cell culture inserts under light stress. Culture medium with thiamine was used as a control. Treatment with oxythiamine significantly increased the number of TUNEL positive cells under light stress compared with the thiamine treatment group (Fig. 6C–D).

4. Discussion

The PPP is a major regulator of cellular reduction-oxidation (redox) homeostasis and biosynthesis [13]. To explore the role of the PPP in the human retina, the expression and function of TKT, a critical PPP enzyme, were studied. Immunofluorescent staining of human neural retinal sections found that TKT was predominantly expressed in Müller cells (Fig. 1). We believe that PPP plays an important role in the anti-oxidative function of Müller cells in the retina [23]. We also found that gliotic Müller cells in the retina with AMD expressed less TKT than Müller cells in the normal retina (Fig. 1S). Although we do not know whether this change is the primary effect or the secondary to Müller cell gliosis, this observation suggests that the dysregulation of TKT may be involved in the pathogenesis of AMD.

TKT may contribute to pyruvate production by Müller cells, linking PPP and glycolysis. ¹³C-glucose labelling experiments showed significant changes in pyruvate production by huPMCs following TKT knockdown (Fig. 3). Total pyruvate production decreased, but there was a redistribution of pyruvate isotopologues. Specifically, the level of pyruvate generated from both PPP (M1) and glycolysis (M2) decreased after TKT knockdown. These results were consistent when analysed using either ¹³C enrichment (isotopologue distribution percentage) or pool sizes (metabolite abundance). This suggests that TKT knockdown inhibited PPP activity and reduced overall pyruvate synthesis. Additionally, M2 TCA metabolites, which derive from glycolysis [24], including citrate, aKG, succinate, fumarate and malate, had higher isotopologue distributions in the TKT knockdown group than the control. These results suggest that relatively more glucose enters the TCA cycle directly via glycolysis after TKT knockdown than indirectly via the PPP.

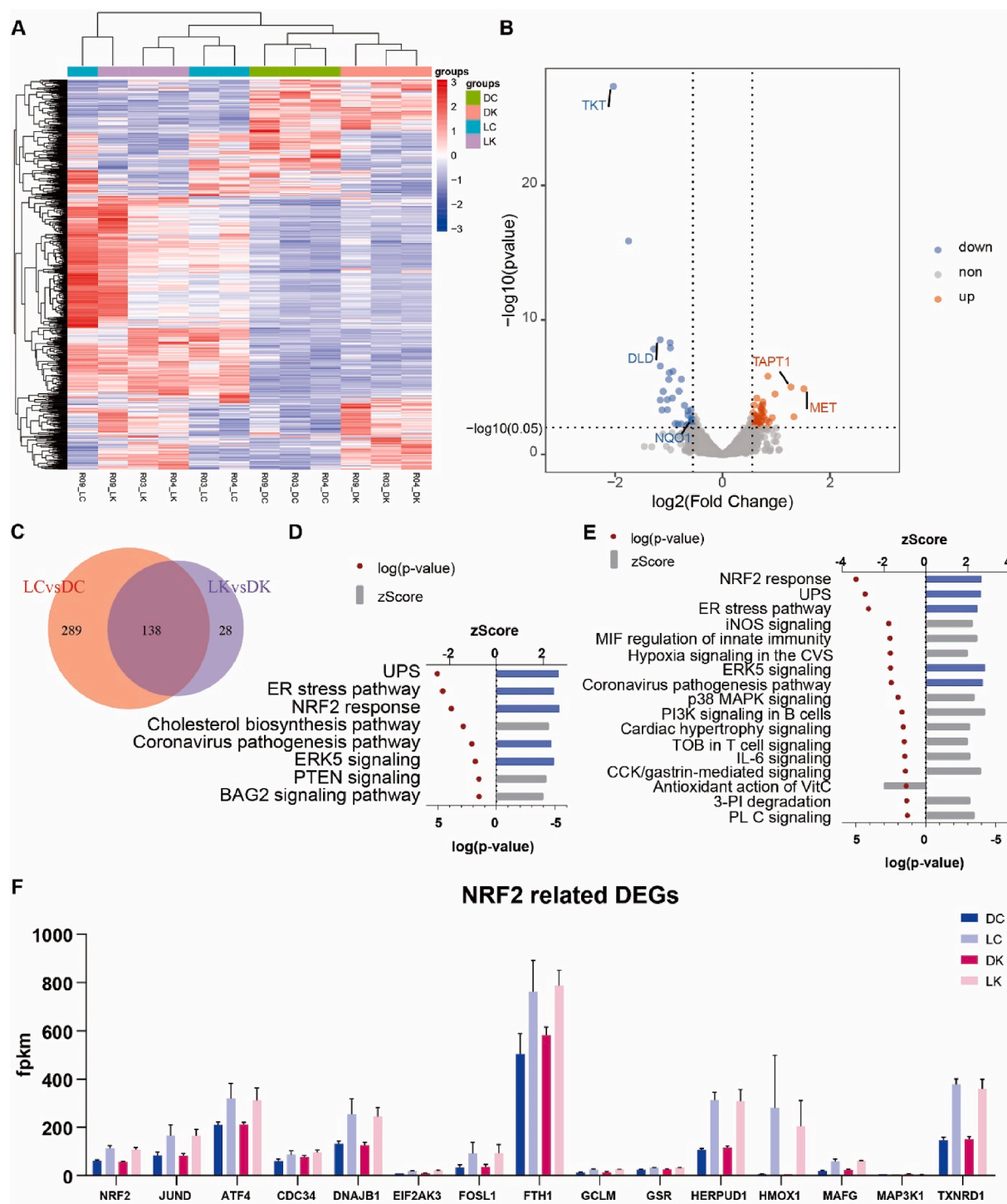


Fig. 4. Transcriptomic analysis of huPMCs after transketolase (TKT) knockdown and light stress. A heatmap of clustered differentially expressed genes (DEGs). Samples were from three donors (R03, R04, R09), shown at the bottom of the heatmap. Each donor had four groups, “dim control” (DC), “dim knockdown” (DK), “light control” (LC), “light knockdown” (LK), shown above. Red indicated a higher expression level, while blue indicated a lower expression level. B volcano plot showing DEGs between “DK vs DC”. Gene fold changes are represented on the horizontal axis, with statistically significant changes on the vertical axis. Individual genes were represented by points (grey, not significant; red, significantly upregulated; blue, significantly downregulated). C Venn chart comparing “LC vs DC” DEGs and “LK vs DK” DEGs. D and E Ingenuity Pathway Analysis (IPA) of “LC vs DC” DEGs and “LK vs DK” DEGs. Pathways that were upregulated or downregulated were represented on the vertical axis. The Z-score was represented on the upper horizontal axis. Red dots indicate the $-\log(p\text{-value})$, with bars representing activated or inhibited pathways unique to each comparison (grey) or common to both (blue). UPS: unfolded protein response; ER: endoplasmic reticulum; CVS: cardiovascular system; CCK: cholecystokinin; VitC: vitamin C; PI: phosphoinositide; PL: phospholipase; F Prominent NRF2 related DEGs. n = 3 per group. Error bars = SEM. (For interpretation of the references to colour in this figure legend, the reader is referred to the Web version of this article.)

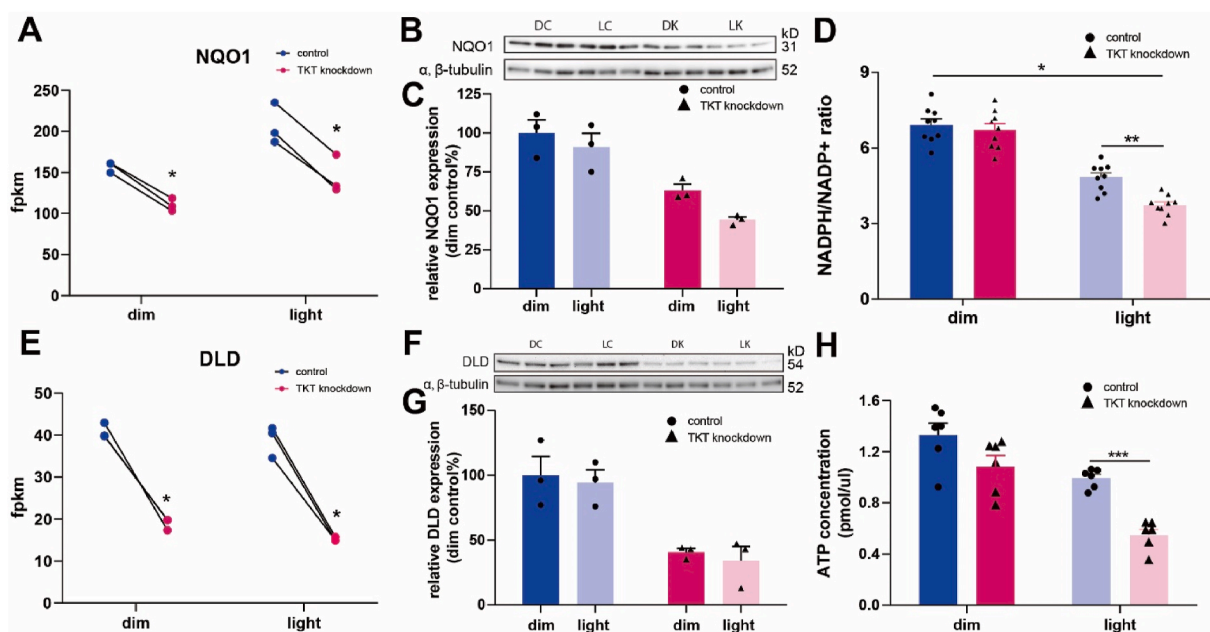


Fig. 5. NQO1, DLD and anti-oxidation responses. A NQO1 mRNA from huPMCs after control or TKT siRNA knockdown treatment followed by bright or dim light exposure. B WB analysis of NQO1 and α/β tubulin in huPMCs after different treatments. C Quantitative analysis of the NQO1 expression in the cells. NQO1 expression level is normalised to α/β tubulin. n = 3 per group. Error bars = SEM. D NADPH/NADP⁺ ratio in huPMCs after different treatments. p-value indicated the significance of the variance contributed by the interaction between TKT and light stress. Comparisons were conducted by two-way ANOVA. n = 9 per group. Error bars = SEM. E DLD mRNA from huPMCs after different treatments. F WB analysis of DLD and α/β tubulin in huPMCs after different kinds of treatments. G Quantitative analysis of the DLD expression in the cells. DLD expression level is normalised to α/β tubulin. n = 3 per group. Error bars = SEM. H ATP concentration in huPMCs after different treatments. Comparisons were conducted by two-way ANOVA. n = 6 per group. Error bars = SEM. *: p < 0.05; **: p < 0.01. ATP: Adenosine triphosphate. DC: dim control, DK: dim knockdown, LC: light control, LK: light knockdown. DLD: Dihydroliipoamide dehydrogenase. Fpkm: Fragments Per Kilobase of transcript per Million mapped reads. HuPMCs: human primary Müller cells. NADPH/NADP⁺: Nicotinamide adenine dinucleotide phosphate. NQO1: NAD(P)H Quinone Dehydrogenase 1. WB: Western blot.

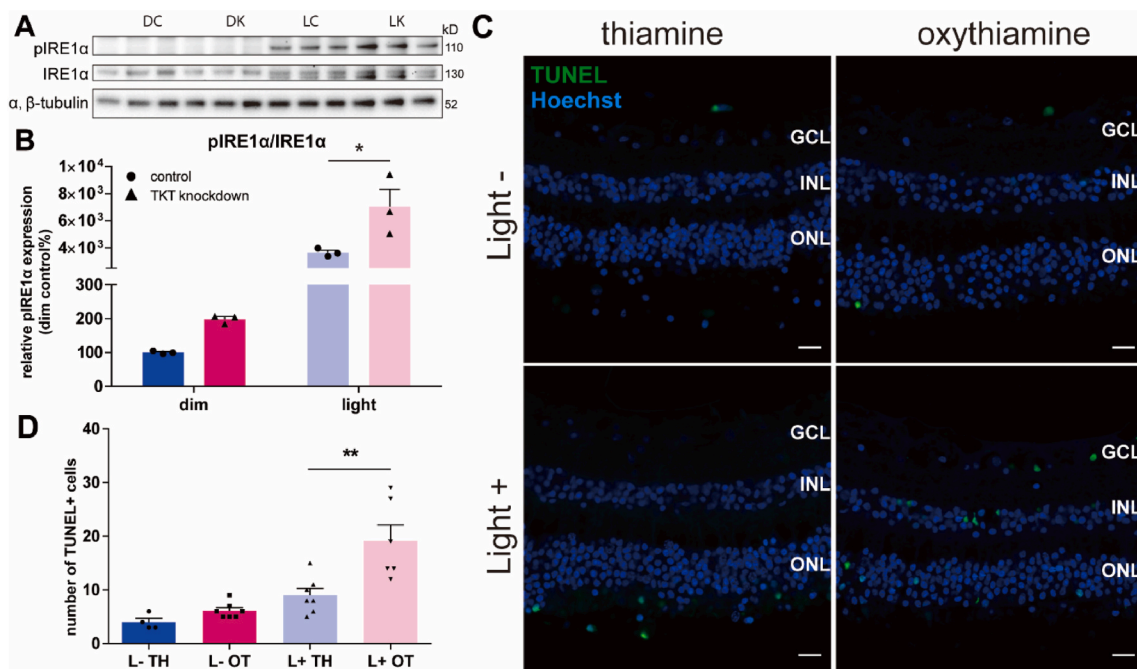


Fig. 6. TKT was critical for ER stress responses and cell survival in the human retina. A, B WB and quantitative analysis of pIRE1 α , IRE1 α , and α/β tubulin expression in huPMCs after TKT knockdown and light stress. The expression level is normalised to IRE1 α . n = 3 per group. *: p < 0.05. Comparisons were conducted by two-way ANOVA. Error bars = SEM. C TUNEL (green) and Hoechst (blue) staining of retinal explant after thiamine or oxythiamine treatment followed by light stress. Scale bars: 20 μ m. GCL: ganglion cell layer. INL: inner nuclear layer. ONL: outer nuclear layer. D Quantitative analysis of the TUNEL staining. **: p < 0.01. Comparisons were conducted by one-way ANOVA. n = 4–7 per group. Error bars = SEM. DC: dim control, DK: dim knockdown, LC: light control, LK: light knockdown. HuPMCs: human primary Müller cells. OT: oxythiamine, TH: thiamine. WB: Western blot. (For interpretation of the references to colour in this figure legend, the reader is referred to the Web version of this article.)

TKT appears to play a significant role in pyruvate oxidation. Overall, TCA cycle activity was reduced following TKT knockdown, with a significant reduction of abundance in all TCA metabolites analysed (labelled and non-labelled) (Fig. 3E). This should reduce overall oxidative activity following TKT knockdown, which is consistent with the findings of the AlamarBlue assay (Fig. 2J). These results suggest TCA metabolism is impaired by TKT knockdown despite a relative increase in M2 pyruvate entering the TCA cycle. Additionally, TKT knockdown significantly inhibited DLD expression. DLD is part of the E3-harboring multienzyme dehydrogenase complexes for alpha-ketoglutarate: KGDHc, pyruvate: PDHc, alpha-ketoadipate: KADHc, and branched-chain alpha-keto acids: BCKDHc, as well as part of the glycine cleavage system (GCS) [25]. The dehydrogenases participate in pyruvate oxidation, suggesting that reduced DLD contributes to the decrease of ATP levels and metabolic activity that we observed. Metabolic decompensation caused by E3 deficiency may cause neurological symptoms that are often fatal [26]. Reduced DLD can induce autophagic cell death by producing reactive oxygen species (ROS) [27].

Light stress introduces oxidative and mitochondrial insults [28], which may participate in the development of prevalent retinal diseases, including diabetic retinopathy (DR) [29] and age-related macular degeneration (AMD) [30]. Intense light exposure has been reported to induce photoreceptor degeneration and the death of horizontal cells [31]. Light-induced retinal degeneration models share many common pathogenic characteristics with AMD [32]. Models of light exposure have been used to study the regulation of retinal sphingolipids and ER stress in AMD [33,34]. HuPMCs with TKT knockdown were exposed to light stress to study further the roles of TKT in the Müller cells' response to stress (Fig. 2). TKT knockdown alone did not result in significant changes, but it played a synergistic role that exacerbated the effect of the light stress, which caused reduced total metabolic activity (Fig. 2J), NADPH/NADP⁺ ratios (Fig. 5D), ATP levels (Fig. 5G), and aggravated ER stress induced by intense light (Fig. 6B). Furthermore, inhibition of TKT with oxythiamine [18], increased the number of TUNEL positive cells in the human retina (Fig. 6C, D). This suggests that the PPP plays a critical protective role in the stressed retina.

TKT knockdown rendered huPMCs more susceptible to light stress. Light stress inhibited TKT enzyme activity (Fig. 2H) but, surprisingly, slightly increased TKT mRNA levels. The Alamarblue assay found that the overall metabolic activity of huPMCs was inhibited by intense light exposure (Fig. 2J). There were no significant differences in LDH levels between the different treatment groups, suggesting the metabolic differences were not caused by cell death. The inhibition of overall metabolic activity caused by light stress was exacerbated by TKT knockdown (Fig. 2J), likely by inhibition of pyruvate oxidation (Fig. 3C). This deleterious effect of TKT knockdown on cell function likely accumulates over time, particularly during times of retinal stress, ultimately causing retinal disease.

PPP disruption contributes to the decreased capacity of Müller cells to maintain redox homeostasis in the retina under light stress. Müller cells depend on NADPH to generate glutathione, the major retinal antioxidant [35]. The generation of NADPH relies on both the PPP and NAD⁺, which is a cofactor in antioxidant systems [36]. Disturbance of either PPP by TKT knockdown or NAD⁺ by inhibition of pyruvate oxidation could reduce the level of NADPH.

NRF2, which is sensitive to the redox state, regulates the transcription of antioxidative genes [37]. The IPA analysis based on the RNAseq data found "NRF2-Mediated Oxidative Stress Response" was top-ranked when comparing normal and light-stressed conditions after TKT had been knocked down. The NRF2 response only ranked third when TKT expression was normal. This finding indicates that oxidative stress was elevated in Müller cells when TKT was knocked down. NQO1 is one of the key genes downstream of the NRF2 pathway and is essential for anti-oxidation [38]. TKT knockdown decreased both mRNA and protein levels of NQO1 (Fig. 5). This would be expected to weaken cells' ability to combat oxidative stress [39]. Protein levels of NQO1 were not

elevated after light stress, unlike mRNA, possibly because *de novo* protein synthesis lagged behind the relatively rapid consumption of NQO1.

TKT was primarily expressed in the nuclei of Müller cells in the human retina and in primary culture (Figs. 1 and 2C), suggesting it has roles in gene regulation in addition to its enzymatic function in Müller cells. Recent studies have suggested that essential glycolytic enzymes can be found in the nucleus when cells are facing a changing environment (e.g., development, stem cell differentiation), where translocation of the enzymes to the nucleus facilitates adaptation to stress [40]. Metabolic enzymes in the nucleus can also participate in tumour progression independent of their canonical metabolic roles [41]. These multifaceted glycolytic enzymes directly link metabolism to epigenetic and transcription programs implicated in tumorigenesis [41]. A recent cross-linking Co-IP/MS study found that nuclear TKT interacted with kinases and transcriptional coregulators, such as EGFR and ERK, associated with cell activation or stress response processes [16]. DLD is the common component of the three alpha-ketoacid dehydrogenase complexes that oxidise pyruvate, alpha-ketoglutarate and the branched-chain alpha-ketoacids, performing a vital role in energy metabolism [42]. DLD and NQO1 mRNA changes in this study were analysed after TKT knockdown. The non-canonical regulatory function of TKT likely caused these downstream changes since DLD expression has been reported to respond to manipulation of MAPK signalling [43]. In contrast, the NRF2 pathway, which regulates NQO1 expression, can also be controlled by EGFR [44]. The mechanism of how TKT regulates the expression of NQO1 and DLD warrants further investigation.

We found that TKT knockdown reduced the expression of DLD and NQO1 and the synthesis and oxidation of pyruvate. TKT knockdown in the light-stressed retina resulted in a significant reduction in cellular ATP, glucose metabolism and NADPH/NADP⁺ ratios, which was associated with disturbed energy supply and redox balance and rendered cells more vulnerable to oxidative stress (Fig. 7). Oxidative stress is considered a primary contributor to the pathologic changes in diabetic retinopathy [29]. Recent findings suggest that the macula consumes more pyruvate than the peripheral retina [20]. Thus we speculate that the macula is more vulnerable to energy deficiency following disruption of the PPP. Boosting TKT may potentially maintain and even restore redox balance in the retina. Thiamine, vitamin B1, is the TKT co-enzyme that enhances its activity. Benfotiamine (BFT), a lipid-soluble derivative of thiamine with faster absorption and better bioavailability [45], has been studied in the treatment of diabetic neuropathy [46]. Although the therapeutic potential of BFT in DR has been reported in a study *in vitro* [47], further investigations are needed to evaluate if it can combat DR *in vivo*. Further research is warranted to identify whether manipulation of TKT might represent an effective way to treat retinal conditions characterised by excessive oxidative stress and/or metabolic derangement, such as diabetic retinopathy.

5. Conclusions

We found that TKT had both canonical metabolic functions and non-canonical regulatory functions in human Müller cells. The dysfunction of TKT constrained the PPP and decreased the *de novo* synthesis of pyruvate. This led to derangement of the TCA cycle and ATP level decrease that threatened the energy supply. TKT also down-regulated the expression of NQO1 and DLD in Müller cells. The metabolic functions and gene-regulation functions of TKT appear to be critical for the maintenance of Müller cell homeostasis.

Author contribution

T.Z., L.Z., J.D., M.G. designed the study; Y.-C., T.Z., S.Z., R.X., Y.-W., M.Z. S.L., M.Y. carried out the experiment; Y.-C., T.Z., J.D., X.F., K.J., S.L. analysed the data. Y.C., L.Z., T.Z. wrote the manuscript; J.D., M.G., N.-C., M.Z., K.-W., A.C. revised the manuscript critically. All authors approved the final version to be published and agree to be accountable for all

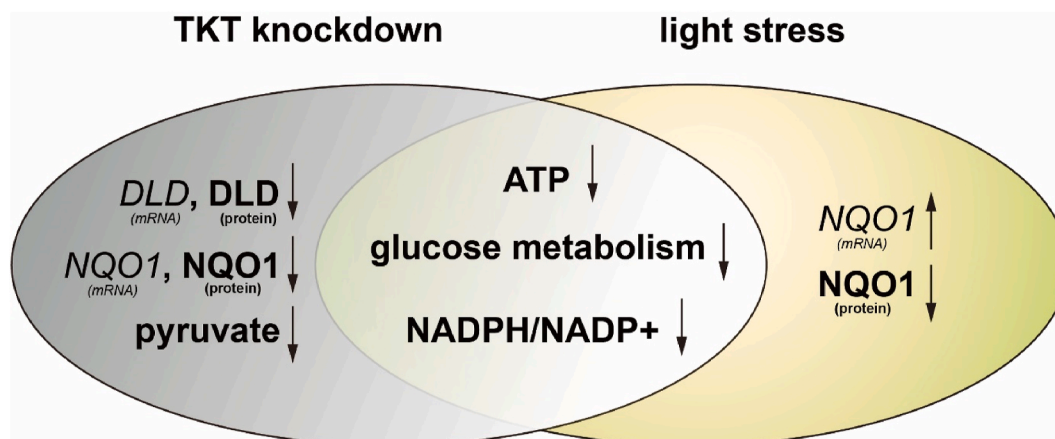


Fig. 7. A summary of factors involved in TKT knockdown and light stress. TKT knockdown decreased the mRNA and the protein level of both DLD and NQO1. TKT knockdown also inhibited pyruvate synthesis and oxidation. Light stress increased NQO1 mRNA level as a response to oxidative stress. The protein level of NQO1 decreased after a short time of exposure to light. Taken together, TKT knockdown and light stress contributed to the drop of cellular ATP level, glucose metabolism and NADPH/NADP⁺ ratio. ATP: Adenosine triphosphate. DLD: Dihydroliipoamide dehydrogenase. NADPH/NADP⁺: Nicotinamide adenine dinucleotide phosphate. NQO1: NAD(P)H Quinone Dehydrogenase 1. TKT: transketolase.

aspects of the work in ensuring that questions related to the accuracy or integrity of any part of the work are appropriately investigated and resolved.

Declaration of competing interest

The authors declare that they have no conflict of interest.

Acknowledgement

All the human eye tissues used in this study were from the New South Wales Tissue Bank distributed through the Australian Ocular Biobank. We thank the eye donors and their families for their contribution and acknowledge the staff members in the Tissue Bank and Ocular Biobank for the tissue supply. This study was supported by the Ophthalmic Research Institute of Australia (TZ, MG), the National Health and Medical Research Council (Investigator Grant GNT_1195021) (MG), the Lowy Medical Research Institute (MG, LZ, TZ), the Partnership Collaboration Award (USYD-ZJU) (LZ, XF), and the National Eye Institute (EY032462, EY031324) (JD).

Appendix A. Supplementary data

Supplementary data to this article can be found online at <https://doi.org/10.1016/j.redox.2022.102379>.

References

- [1] A. Reichenbach, A. Bringmann, Glia of the human retina, *Glia* 68 (4) (2020) 768–796.
- [2] A. Reichenbach, A. Bringmann, New functions of Muller cells, *Glia* 61 (5) (2013) 651–678.
- [3] N.J. Coorey, W. Shen, S.H. Chung, L. Zhu, M.C. Gillies, The role of glia in retinal vascular disease, *Clin. Exp. Optom.* 95 (3) (2012) 266–281.
- [4] M.R. Verardo, G.P. Lewis, M. Takeda, K.A. Linberg, J. Byun, G. Luna, et al., Abnormal reactivity of muller cells after retinal detachment in mice deficient in GFAP and vimentin, *Invest. Ophthalmol. Vis. Sci.* 49 (8) (2008) 3659–3665.
- [5] B.A. Coughlin, D.J. Feenstra, S. Mohr, Muller cells and diabetic retinopathy, *Vis. Res.* 139 (2017) 93–100.
- [6] D.V. Telegina, O.S. Kozhevnikova, N.G. Kolosova, Changes in retinal glial cells with age and during development of age-related macular degeneration, *Biochemistry (Mosc.)* 83 (9) (2018) 1009–1017.
- [7] Y. You, L. Zhu, T. Zhang, T. Shen, A. Fontes, C. Yiannikas, et al., Evidence of muller glial dysfunction in patients with aquaporin-4 immunoglobulin G-positive neuromyelitis optica spectrum disorder, *Ophthalmology* 126 (6) (2019) 801–810.
- [8] M.B. Powner, M.C. Gillies, M. Zhu, K. Vevis, A.P. Hunyor, M. Fruttiger, Loss of Muller's cells and photoreceptors in macular telangiectasia type 2, *Ophthalmology* 120 (11) (2013) 2344–2352.
- [9] R.L. Pfeiffer, R.E. Marc, M. Kondo, H. Terasaki, B.W. Jones, Muller cell metabolic chaos during retinal degeneration, *Exp. Eye Res.* 150 (2016) 62–70.
- [10] T. Zhang, M.C. Gillies, M.C. Madigan, W. Shen, J. Du, U. Grunert, et al., Disruption of de novo serine synthesis in muller cells induced mitochondrial dysfunction and aggravated oxidative damage, *Mol. Neurobiol.* 55 (8) (2018) 7025–7037.
- [11] L. Chen, Z. Zhang, A. Hoshino, H.D. Zheng, M. Morley, Z. Arany, et al., NADPH production by the oxidative pentose-phosphate pathway supports folate metabolism, *Nature Metabolism* 1 (3) (2019) 404–415.
- [12] Lt Adler, C. Chen, Y. Koutalos, Mitochondria contribute to NADPH generation in mouse rod photoreceptors, *J. Biol. Chem.* 289 (3) (2014) 1519–1528.
- [13] T. Ge, J. Yang, S. Zhou, Y. Wang, Y. Li, X. Tong, The role of the pentose phosphate pathway in diabetes and cancer, *Front. Endocrinol.* 11 (2020) 365.
- [14] N. Tian, Q. Liu, Y. Li, L. Tong, Y. Lu, Y. Zhu, et al., Transketolase deficiency in adipose tissues protects mice from diet-induced obesity by promoting lipolysis, *Diabetes* 69 (7) (2020) 1355–1367.
- [15] K.C. Patra, N. Hay, The pentose phosphate pathway and cancer, *Trends Biochem. Sci.* 39 (8) (2014) 347–354.
- [16] Z. Qin, C. Xiang, F. Zhong, Y. Liu, Q. Dong, K. Li, et al., Transketolase (TKT) activity and nuclear localization promote hepatocellular carcinoma in a metabolic and a non-metabolic manner, *J. Exp. Clin. Cancer Res.* 38 (1) (2019) 154.
- [17] M. Zhao, M. Ye, J. Zhou, X. Zhu, Prognostic values of transketolase family genes in ovarian cancer, *Oncol. Lett.* 18 (5) (2019) 4845–4857.
- [18] C.W. Tseng, W.H. Kuo, S.H. Chan, H.L. Chan, K.J. Chang, L.H. Wang, Transketolase regulates the metabolic switch to control breast cancer cell metastasis via the alpha-ketoglutarate signaling pathway, *Cancer Res.* 78 (11) (2018) 2799–2812.
- [19] Y. Chen, T. Zhang, S. Zeng, M. Yam, M.C. Gillies, L. Zhu, Isolation, culture, and identification of primary muller cells from human retina, *Bio Protoc* 11 (19) (2021), e4179.
- [20] B. Li, T. Zhang, W. Liu, Y. Wang, R. Xu, S. Zeng, et al., Metabolic features of mouse and human retinas: rods versus cones, macula versus periphery, retina versus RPE, *iScience* 23 (11) (2020), 101672.
- [21] P. Millard, B. Delepine, M. Guionnet, M. Heuillet, F. Bellvert, F. Leticie, IsoCor: isotope correction for high-resolution MS labeling experiments, *Bioinformatics* 35 (21) (2019) 4484–4487.
- [22] T. Mao, M. Shao, Y. Qiu, J. Huang, Y. Zhang, B. Song, et al., PKA phosphorylation couples hepatic inositol-requiring enzyme 1 alpha to glucagon signaling in glucose metabolism, *Proc. Natl. Acad. Sci. U. S. A.* 108 (38) (2011) 15852–15857.
- [23] K. Eastlake, J. Luis, G.A. Limb, Potential of muller glia for retina neuroprotection, *Curr. Eye Res.* 45 (3) (2020) 339–348.
- [24] S. Diaz-Moralli, E. Aguilar, S. Marin, J.F. Coy, M. Dewerchin, M.R. Antoniewicz, et al., A key role for transketolase-like 1 in tumor metabolic reprogramming, *Oncotarget* 7 (32) (2016) 51875–51897.
- [25] A. Ambrus, An updated view on the molecular pathomechanisms of human dihydroliipoamide dehydrogenase deficiency in light of novel crystallographic evidence, *Neurochem. Res.* 44 (10) (2019) 2307–2313.
- [26] A. Ambrus, V. Adam-Vizi, Human dihydroliipoamide dehydrogenase (E3) deficiency: novel insights into the structural basis and molecular pathomechanism, *Neurochem. Int.* 117 (2018) 5–14.
- [27] S. Yumnam, M.C. Kang, S.H. Oh, H.C. Kim, J.C. Kim, E.S. Jung, et al., Downregulation of dihydroliipoamide dehydrogenase by UVA suppresses melanoma progression via triggering oxidative stress and altering energy metabolism, *Free Radic. Biol. Med.* 162 (2021) 77–87.
- [28] L. Trachsel-Moncho, S. Benlloch-Navarro, A. Fernandez-Carbonell, D.T. Ramirez-Lamelas, T. Olivar, D. Silvestre, et al., Oxidative stress and autophagy-related changes during retinal degeneration and development, *Cell Death Dis.* 9 (8) (2018) 812.

- [29] Q. Kang, C. Yang, Oxidative stress and diabetic retinopathy: molecular mechanisms, pathogenetic role and therapeutic implications, *Redox Biol.* 37 (2020), 101799.
- [30] S. Beatty, H. Koh, M. Phil, D. Henson, M. Boulton, The role of oxidative stress in the pathogenesis of age-related macular degeneration, *Surv. Ophthalmol.* 45 (2) (2000) 115–134.
- [31] M. Samardzija, V. Todorova, L. Gougoulakis, M. Barben, S. Notzli, K. Klee, et al., Light stress affects cones and horizontal cells via rhodopsin-mediated mechanisms, *Exp. Eye Res.* 186 (2019), 107719.
- [32] M.D. Marquioni-Ramella, A.M. Suburo, Photo-damage, photo-protection and age-related macular degeneration, *Photochem. Photobiol. Sci.* 14 (9) (2015) 1560–1577.
- [33] R. Terao, M. Honjo, T. Ueta, H. Obinata, T. Izumi, M. Kurano, et al., Light stress-induced increase of sphingosine 1-phosphate in photoreceptors and its relevance to retinal degeneration, *Int. J. Mol. Sci.* 20 (15) (2019).
- [34] J.Y. Song, B. Fan, L. Che, Y.R. Pan, S.M. Zhang, Y. Wang, et al., Suppressing endoplasmic reticulum stress-related autophagy attenuates retinal light injury, *Aging (Albany NY)* 12 (16) (2020) 16579–16596.
- [35] D. Huster, A. Reichenbach, W. Reichelt, The glutathione content of retinal Muller (glial) cells: effect of pathological conditions, *Neurochem. Int.* 36 (4–5) (2000) 461–469.
- [36] W. Xiao, R.S. Wang, D.E. Handy, J. Loscalzo, NAD(H) and NADP(H) redox couples and cellular energy metabolism, *Antioxidants Redox Signal.* 28 (3) (2018) 251–272.
- [37] T. Nguyen, P. Nioi, C.B. Pickett, The Nrf2-antioxidant response element signaling pathway and its activation by oxidative stress, *J. Biol. Chem.* 284 (20) (2009) 13291–13295.
- [38] D. Ross, D. Siegel, Functions of NQO1 in cellular protection and CoQ10 metabolism and its potential role as a redox sensitive molecular switch, *Front. Physiol.* 8 (2017) 595.
- [39] S. Luo, S.S. Kang, Z.H. Wang, X. Liu, J.X. Day, Z. Wu, et al., Akt phosphorylates NQO1 and triggers its degradation, abolishing its antioxidative activities in Parkinson's disease, *J. Neurosci.* 39 (37) (2019) 7291–7305.
- [40] A.E. Boukouris, S.D. Zervopoulos, E.D. Michelakis, Metabolic enzymes moonlighting in the nucleus: metabolic regulation of gene transcription, *Trends Biochem. Sci.* 41 (8) (2016) 712–730.
- [41] X. Yu, S. Li, Non-metabolic functions of glycolytic enzymes in tumorigenesis, *Oncogene* 36 (19) (2017) 2629–2636.
- [42] D.J. Carothers, G. Pons, M.S. Patel, Dihydroliipoamide dehydrogenase: functional similarities and divergent evolution of the pyridine nucleotide-disulfide oxidoreductases, *Arch. Biochem. Biophys.* 268 (2) (1989) 409–425.
- [43] G. Zhang, L.S. He, Y. Him Wong, Y. Xu, Y. Zhang, P.Y. Qian, p38 MAPK regulates PKAalpha and CUB-serine protease in *Amphibalanus amphitrite* cyprids, *Sci. Rep.* 5 (2015), 14767.
- [44] T. Ishii, E. Warabi, Mechanism of rapid nuclear factor-E2-related factor 2 (Nrf2) activation via membrane-associated estrogen receptors: roles of NADPH oxidase 1, neutral sphingomyelinase 2 and epidermal growth factor receptor (EGFR), *Antioxidants* 8 (3) (2019).
- [45] V. Raj, S. Ojha, F.C. Howarth, P.D. Belur, S.B. Subramanya, Therapeutic potential of benfotiamine and its molecular targets, *Eur. Rev. Med. Pharmacol. Sci.* 22 (10) (2018) 3261–3273.
- [46] D. Ziegler, N. Papanas, O. Schnell, B.D.T. Nguyen, K.T. Nguyen, K. Kulkantrakorn, et al., Current concepts in the management of diabetic polyneuropathy, *J Diabetes Investig* 12 (4) (2021) 464–475.
- [47] H.P. Hammes, X. Du, D. Edelstein, T. Taguchi, T. Matsumura, Q. Ju, et al., Benfotiamine blocks three major pathways of hyperglycemic damage and prevents experimental diabetic retinopathy, *Nat. Med.* 9 (3) (2003) 294–299.